Source Characterization by the Allan Variance

C. Gattano, S. Lambert

Abstract Until now, the main criteria for selecting geodetic sources were based on astrometric stability and structure at 8 GHz [6]. But with more observations and the increase of accuracy, the statistical tools used to determine this stability become inappropriate with regards to sudden motions of the radiocenter. In this work, we propose to replace these tools by the Allan Variance [1], first used on VLBI sources by M. Feissel-Vernier [3], leading to a new classification of sources into three groups according to the shape of the Allan Variance. In parallel, we combine two catalogs, the Large Quasar Astrometric Catalogue [13] and the Optical Characteristics of Astrometric Radio Sources [10], in order to gather most physical characteristics known about these VLBI targets. By doing so, we may reveal physical criteria that may be useful in the selection of new targets for future VLBI observations.

Keywords VLBI, Allan Variance, source stability, source classification

1 Introduction

The need for stable sources on the celestial sphere has existed for a long time, because they are used to materialize a non-rotating universe around the Earth and realize a so-called quasi-inertial reference frame. Such a frame is fundamental, because the physical laws are expressed only through it—otherwise inertial forces have to be applied to explain observed motions. One principal application of the celestial reference frames is the study of the Earth orientation parameters (EOP), five in total, which characterize the change of Earth orientation with respect to the non-rotating universe due to solar system objects' attraction and to geophysical response.

In 1999, the commonly approved celestial reference frame (CRF) changed from a catalog of stars to a catalog of extragalactic objects seen through Very Long Baseline Interferometry (VLBI), the ICRF1 [9]. During its construction, a particular interest was put on the selection of the defining sources (DS), which are the most stable sources that carry the axes of the frame. The method used was based on arbitrary thresholds of observation time history and uncertainties of position adjustments through VLBI analysis. Then, a source was rejected if it showed significant position differences when two random subsets were statistically oriented in the same directions. Sources presenting a non-linear motion or a large source structure were also rejected. By doing so, 212 DS were selected out of 608 sources. A first extension added 59 sources to the catalog. A second extension added 109, and the DS subset was reconsidered to 207 [5].

In 2001, Gontier et al. [7] investigated the stability of the CRF and produced an automatic algorithm to iteratively deselect sources from the DS subset based on the time behavior and statistical approach. They got 242 DS for their most stable frame. In 2003, Feissel-Vernier [3] introduced the use of the Allan Variance in conjunction with the observation history and linear drift. She obtained 199 DS, and in 2006 an extension was released based on this method, in order to increase the number of DS [4]. This extension competed with ICRF work.

SYRTE, Observatoire de Paris, PSL Research University, CNRS, Sorbonne Universités, UPMC Univ.

In 2009, the second realization of the ICRF [6] was released based on a method close to the ICRF1 approach but taking the time behavior into account. However, in the process the Allan Variance was replaced by the classical variance of the position time series. In this context, it can also be noted that one improvement of the ICRF2 was to take into account the declination coverage in the DS subset.

Since then, the ICRF2 has been used as reference frame. But seven years have passed, new source observations have been added to the observational history, and no study has been presented to refine the DS subset with respect to stability. It is obvious that things must have changed, and we propose here to again use the Allan Variance to determine the stability of the VLBI sources with more than 100 observing sessions, i.e., 202 sources, and select the stable ones. In Section 2, we explain the principle of the Allan Variance and its modified form. In Section 3, we present its application to the 202 most observed VLBI sources and detail the three subsets based on Allan Variance tendencies. In Section 4, we analyze our results together with the physical characteristics from the Large Quasar Astrometric Catalogue (LQAC [13]) and the Optical Characteristics of Astrometric Radio Sources (OCARS [10]), and finally we draw some conclusions.

2 The Tool: Allan Variance

A. Regular sampling of the function with a minimal time scale τ

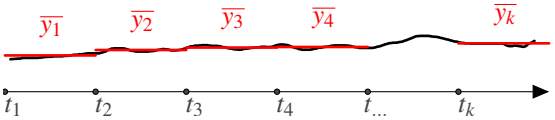

B. Applying the Allan Variance equation

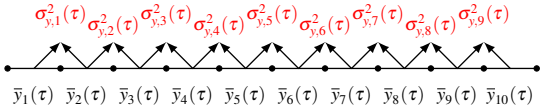

C. Increasing the time scale $\tau \rightarrow 2\tau$ and applying the Allan Variance again

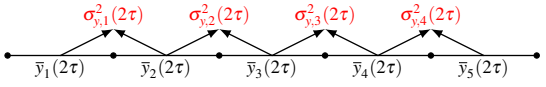

D. Further increasing the time scale

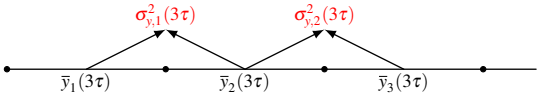

E. Average all $\sigma^2_{y,i}(k\tau)$ for each time scale $k\tau$

Let $y(t)$ be a continuous time function. Given a time scale τ, samples can be computed using

$$\overline{y_k} = \overline{y(t_k)} = \frac{1}{\tau} \int_{t_k}^{t_k+\tau} y(u)du$$

In the case of VLBI data $\overline{y_k}$ is obtained by averaging the observations inside a sliding window of width τ, using as weights the squares of the formal uncertainties.

The Allan Variance [1] is a statistical tool that can study the dispersion of a signal between peers:

$$\sigma^2_y(\tau) = \frac{1}{2} \left\langle (\bar{y}_{k+1} - \bar{y}_k)^2 \right\rangle \quad (1)$$

Rather than study the dispersion around the mean, as with the true variance, we study the variation between two successive samples given a time sampling $k\tau$.

Table 1 Connection between the type of noise, its spectral density behavior, and the Allan Variance tendency.

White noise	$\Rightarrow S_y(f) \propto f^0$	$\Rightarrow \sigma^2_y(\tau) \propto \tau^{-1}$
Flicker noise	$\Rightarrow S_y(f) \propto f^{-1}$	$\Rightarrow \sigma^2_y(\tau) \propto \tau^0$
Random Walk noise	$\Rightarrow S_y(f) \propto f^{-2}$	$\Rightarrow \sigma^2_y(\tau) \propto \tau^{+1}$

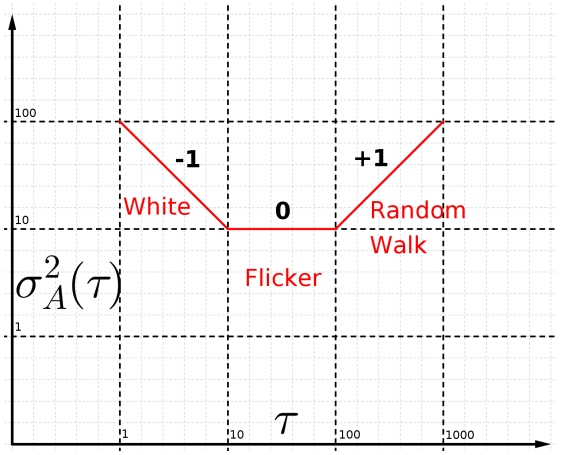

Fig. 1 Allan Variance tendencies with respect to the type of noise.

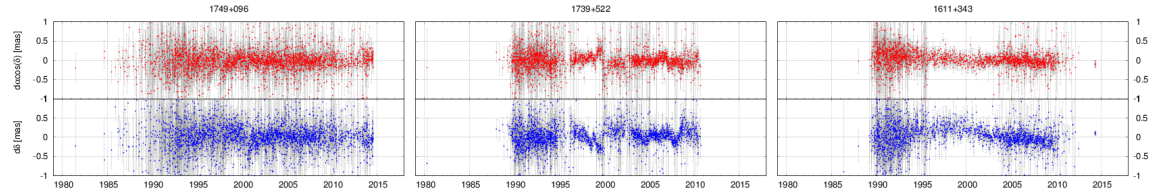

Fig. 2 Examples of radio source coordinate time series from CALC/SOLVE VLBI data analysis. The upper graph shows $d\alpha\cos(\delta)$ with respect to the temporal mean position, while the lower graph shows $d\delta$ with respect to the mean position.

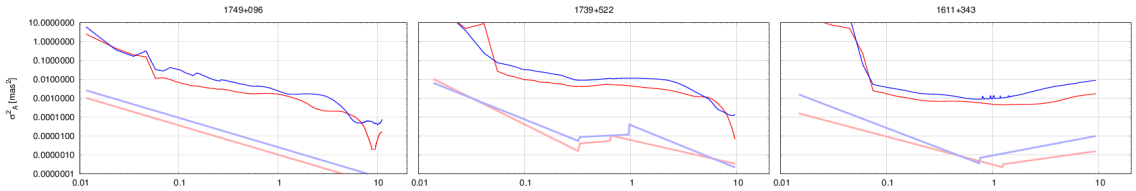

Fig. 3 Allan Variance in $d\alpha\cos(\delta)$ in red (lighter lines) and $d\delta$ in blue (darker lines) of the previous sources and their linear piece-wise adjustment (from left to right): Allan 0 example, Allan 1 example, and Allan 2 example.

VLBI time series can show several types of noise from white noise (or thermal noise) to colored noise such as flicker noise (random jump at random time) and random walk noise. These noise types differ in their spectral density $S_y(f)$ by a different exponent in the power law that leads to different behavior of the Allan Variance.

It is to be noted that in this work we used the modified Allan Variance with the particularity that we do not fill the observation gaps present in most of the time series.

$$ {}^{mod}\sigma_y^2(n\tau) = \frac{1}{2n^4(M-3n+2)} \times \sum_{j=1}^{M-3n+2} \left\{ \sum_{i=j}^{j+n-1} \left(\sum_{k=i}^{i+n-1} \bar{y}_{k+n} - \bar{y}_k \right) \right\}^2 \quad (2) $$

3 The Coordinates Time Series

In order to study the stability of the VLBI radio sources, we worked on the coordinate time series of those targets. We used CALC/SOLVE to analyze all the VLBI non-Intensive sessions available from the IVS Data Centers, and we applied a special treatment to get the time series rather than obtaining them from the independent solution mode.

We obtained time series from ten different solutions where 9/10 of the sources are estimated globally (i.e., one position for all sessions) and 1/10 locally (i.e., one position per session). These ratios were applied separately to defining sources and standard sources (others except the non-linear ones) in order to keep the no-net-rotation constraint (NNR) on 9/10 of the ICRF2 defining sources for a solution with a common subset of at least 8/10 DS when we compare two solutions. A supplementary solution, similar to a typical CRF solution from IVS analysis, enables us to get time series for 39 non-linear sources (NL).

In Figure 2, we show examples of three most observed VLBI sources: 1749+096, 1739+522, and 1611+343. The red (lighter) points are offset in $\alpha\cos\delta$ from the mean position, and the blue (darker) points are offset in δ.

4 Results

We applied the Allan Variance (AV) to VLBI sources present in more than 100 sessions after removing outliers. Then, we modeled AV tendencies by linear piece-wise functions between local minima and maxima. In Figure 3, we show the results for our three examples. AV tendencies are down-shifted, represented by straight red (lighter) lines for $\alpha\cos\delta$ and by blue (darker) lines for δ.

We defined three subsets characterized by the shape of the AV tendencies. The first case, called Allan 0 (e.g., Figure 3 left), gathers sources with a decreasing behavior with respect to an increasing time scale on both $\alpha\cos\delta$ and δ data. It means that we increase the

accuracy of position adjustment if we take into account more and more observations. Such sources are the most suited to define axes of a CRF.

The second case, Allan 1 (e.g., Figure 3 middle), gathers sources that keep a decreasing behavior for a large time scale but at lower ones show a reverse tendency and therefore a degradation of the dispersion on position. It means that the sources have presented some sort of motion, but if we take a sufficiently large observation time range, the phenomenon is averaged, and we get improvements back on position adjustment accuracy. Because of the motion, their usefulness for defining the frame axes is questionable.

The last case and the worst one, called Allan 2 (e.g., Figure 3 right), gathers sources that present an increasing tendency over large time scales. For those sources, adding observations foretell a degradation of the accuracy of its adjustment, and such sources seem not suited for defining the axes of a frame.

In the case of getting different statuses from $\alpha \cos \delta$ and δ, the worst one is selected and associated with the source. In Figure 4, we resume the classification of our sample. A score is also determined by the quadratic sum of the global minima of the Allan Variance in both coordinates, in order to sort them inside each group.

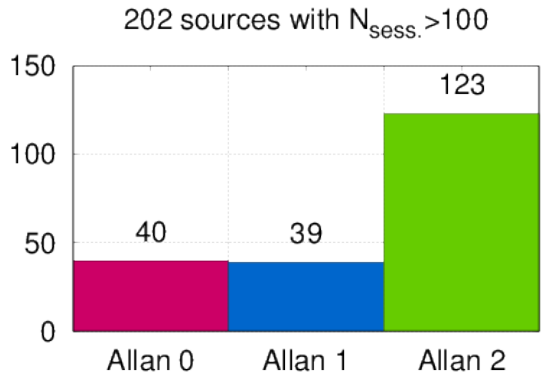

Fig. 4 Number of sources with more than 100 observing sessions in each category in our new classification w.r.t. stability.

5 Analysis and Discussion

In Figure 5, we present the comparison of our classification with respect to the ICRF2 repartition: defining sources (DS), non-linear sources (NL), other sources (Std). In Figure 6, the comparison is made with respect to the redshift taken from the third version of the LQAC [13], which is a compilation of large quasar surveys for several parts of the sky. Note that not all VLBI source redshifts are known. And then, Figure 7 shows the result of the comparison with respect to the type of the object taken from OCARS [10].

The first thing to notice is that this new classification seems not to be in agreement with the repartition of the ICRF2. This can be an effect of the new sessions observed between 2010 and 2016, or it can show that one or the other method is not relevant to determine the stability of a radio source. We plan to apply our methodology to the ICRF2 data, i.e., stop the observation in 2009 in order to conclude if the two methodologies are truly different.

On the other hand, we see that stability with respect to the Allan Variance does not show a dependence on the type of the AGN, i.e., on different orientations of the sources with respect to the line of sight [2, 14]. There may be a dependence on redshift with an optimum between 1 and 2, but it is difficult to conclude because of the low number of sources with redshift greater than 2. Nevertheless, this is not a surprise because cosmology theory tells us that at some redshift, the angular diameter distance of an object increases instead of decreases [8]. For an Einstein-de-Sitter model, the value is between 1 and 1.5.

The stability of the sources may be strongly linked to what happens around the black hole(s), resulting in (multiple-)core emission or (multiple-)beam emission as it is, for instance, shown by the numerical model of Roland et al. [11]. An instability may be seen directly in the observations by the luminous variability of the radio-center, explained in detail by Shabala et al. [12].

6 Conclusions

This work introduces a method to classify VLBI sources by means of the Allan Variance. The result is in disagreement with the ICRF2 classification with regard to stability, and we have to understand why. It could be a divergence between methodologies, or it could be a consequence of the new observations from 2010 to 2016 not available at the time of the ICRF2. We do not succeed in finding a common physical characteristic, especially on the type of the source,

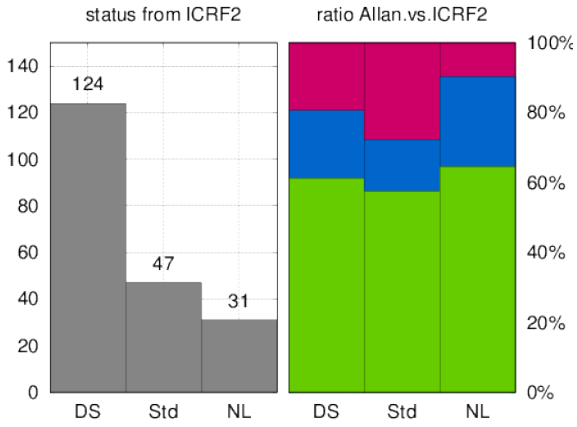

Fig. 5 Repartition of our new classification with respect to the ICRF2 classification: histogram (left); ratio (right). DS = defining sources, Std = standard sources, NL = non-linear sources.

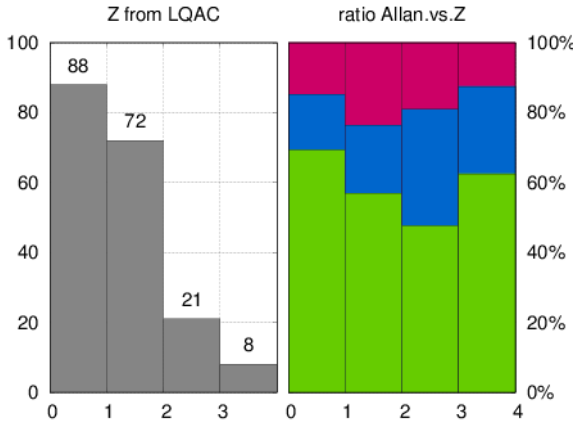

Fig. 6 Repartition of our new classification with respect to the redshift: histogram (left); ratio (right).

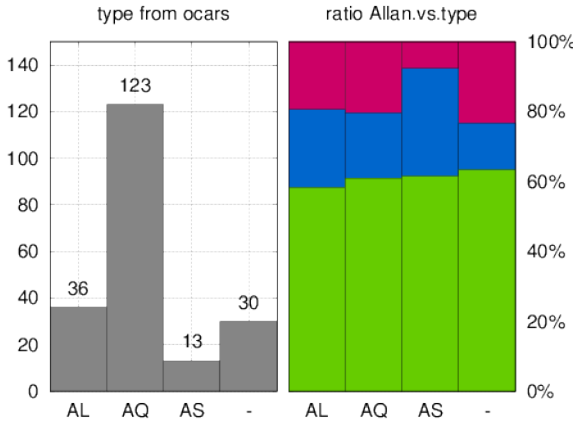

Fig. 7 Repartition of our new classification w.r.t. the type of Active Galactic Nuclei: histogram (left); ratio (right). AL = Blazar, AQ = quasar, AS = Seyfert.

whereas it is advised to select BL-Lacs and Blazars as geodetic VLBI targets to get stable sources because of a collimated beam in the line of sight. The study reveals a preferred redshift value of $1 \sim 1.5$ as good targets as the cosmology theory tells us.

In another work presented in these proceedings, we study the effect of using this classification in the selection of defining sources for the celestial reference frame construction.

References

1. D.W. Allan, Statistics of atomic frequency standards, In IEEE Proceedings, 1966, 54, 221–230.
2. R. Antonucci, Unified models for active galactic nuclei and quasars, In Annual Review of Astron and Astrophys, 1993, 31, 473–521.
3. M. Feissel-Vernier, Selecting stable extragalactic compact radio sources from the permanent astrogeodetic VLBI program, In Astronomy and Astrophysics, 2003, 403, 105–110.
4. M. Feissel-Vernier et al., Analysis strategy issues for the maintenance of the ICRF axes, In Astronomy and Astrophysics, 2006, 452, 1107–1112.
5. A.L. Fey et al., The Second Extension of the International Celestial Reference Frame: ICRF-EXT.1, In Astronomical Journal, 2004, 127, 3587–3608.
6. A.L. Fey et al., The Second Realization of the International Celestial Reference Frame by Very Long Baseline Interferometry, In Astronomical Journal, 2015, 150, 58.
7. A.M. Gontier et al., Stability of the extragalactic VLBI reference frame, In Astronomy and Astrophysics, 2001, 375, 661–669.
8. D.W. Hogg, Distance measures in cosmology, In ArXiv Astrophysics e-prints, 1999.
9. C. Ma et al., The International Celestial Reference Frame as Realized by Very Long Baseline Interferometry, In Astronomical Journal, 1998, 116, 516–546.
10. Z. Malkin, Optical Characteristics of Astrometric Radio Sources OCARS, In Izvestiia Glavnoi rossiiskoi astronomicheskoi observatorii, 2013, 220, 507–510.
11. J. Roland et al., Structure of the nucleus of 1928+738, In Astronomy and Astrophysics, 2015, 578, A86.
12. S.S. Shabala et al., The effects of frequency-dependent quasar variability on the celestial reference frame, In Journal of Geodesy, 2014, 88, 575–586.
13. J. Souchay et al., The third release of the Large Quasar Astrometric Catalog (LQAC-3): a compilation of 321 957 objects, In Astronomy and Astrophysics, 2015, 583, A75.
14. C.M. Urry, P. Padovani, Unified Schemes for Radio-Loud Active Galactic Nuclei, In Publications of the ASP, 1995, 107, 803.